

**Charged lattice gas with a neutralizing background**

V. A. Levashov and M. F. Thorpe

*Department of Physics and Astronomy and Center for Fundamental Materials Research, Michigan State University, East Lansing, Michigan 48824-1116, USA*

B. W. Southern

*Department of Physics and Astronomy, University of Manitoba, Winnipeg, Manitoba, Canada R3T 2N2*

(Received 18 February 2003; published 26 June 2003)

We study a model that was first introduced to describe the ordering of two different types of positive ions in the metal planes of layered hydroxides  $\text{Ni}_{1-x}\text{Al}_x(\text{OH})_2(\text{CO}_3)_{x/2} \cdot y\text{H}_2\text{O}$ . The ordering is assumed to occur due to long-range Coulomb interactions, and overall charge neutrality is provided by a negative background representing the hydroxide planes and  $\text{CO}_3^{2-}$  anions. The previous study was restricted to the ground-state properties. Here we use a Monte Carlo technique to extend the study to finite temperatures. The model predicts that, at some values of the concentration  $x$ , the system can exhibit an instability and phase separate. In order to evaluate the precision of these Monte Carlo procedures, we first study a linear chain with finite-range interactions where exact solutions can be obtained using a transfer-matrix method. For a linear chain with infinite-range interactions, we use a devil's staircase formalism to obtain the dependence of the energy of the equilibrium configurations on  $x$ . Finally we study the two-dimensional triangular lattice using the same Monte Carlo techniques. In spite of its simplicity, the model predicts multiple first-order phase transitions. The model can be useful in applications such as modeling of the ordering of intercalated metal ions in positive electrodes of lithium batteries or in graphite.

DOI: 10.1103/PhysRevB.67.224109

PACS number(s): 61.43.Bn, 64.70.-p, 64.75.+g, 02.70.Uu

**I. INTRODUCTION**

In this paper we continue a study of a model that one of us studied previously.<sup>1</sup> The model was introduced to describe the possible ordering of metal ions that can occur in aluminum-substituted layered nickel double hydroxides  $\text{Ni}_{1-x}\text{Al}_x(\text{OH})_2(\text{CO}_3)_{x/2} \cdot y\text{H}_2\text{O}$ .<sup>2-6</sup>

The Ni ions in  $\text{Ni}(\text{OH})_2$  occupy the octahedral holes between alternate pairs of OH planes and thus form a triangular lattice identical to that adopted by the OH ions. The two planes of OH ions, with the plane of Ni atoms between them, form a brucitelike layer of the host structure.<sup>7</sup>

$\text{Ni}(\text{OH})_2$  can exist in two polymorphous crystal structures denoted as  $\alpha$  and  $\beta$ . Both structures consist of brucitelike layers that are well ordered in the  $\beta$  phase and randomly stacked in the  $\alpha$  phase. The interlayer spacing (gallery) in the  $\alpha$  phase is usually significantly larger than that in the  $\beta$  phase due to the large number of water molecules and anionic species that can penetrate into the galleries.<sup>8</sup>

Nickel hydroxide  $\text{Ni}(\text{OH})_2$  in the  $\beta$  phase has been extensively used as a material for the positive electrode in rechargeable alkaline batteries.<sup>9</sup> However it has been shown that electrodes based on the  $\alpha$ -phase hydroxide have a bigger charge capacity, lower charge, and higher discharge voltages.<sup>10,11</sup> Unfortunately the  $\alpha$  phase reverts to the  $\beta$  phase in the alkaline medium (KOH, for example) which is used in batteries. Thus the stabilization of the  $\alpha$  phase of  $\text{Ni}(\text{OH})_2$  in an alkaline medium is an important goal to reach for use in potential applications. To enhance the  $\text{Ni}(\text{OH})_2$  stability many studies of the partial substitution of metal ions (Al, for example) for Ni in the lattice of nickel hydroxide have been carried out.<sup>12-15</sup>

When  $\text{Ni}^{2+}$  ions are substituted by  $\text{Al}^{3+}$  ions in the metal

sheets,  $[\text{CO}_3]^{2-}$  anions accumulate in the galleries in such an amount that total charge neutrality is preserved. The amount of water in the galleries depends on the preparation method; the general formula of the aluminum-substituted layered nickel hydroxide is  $\text{Ni}_{1-x}\text{Al}_x(\text{OH})_2(\text{CO}_3)_{x/2} \cdot y\text{H}_2\text{O}$ .

It is natural to expect that the stability of these compounds is composition dependent and also depends on the preparation technique. Different authors were able to synthesize layered hydroxides with different concentrations of aluminum. In particular, the range  $0 \leq x \leq 0.4$  has been reported.<sup>7</sup> Not all ranges of composition  $x$  are accessible due to the limited number of  $[\text{CO}_3]^{2-}$  ions and water molecules that can penetrate into the gallery.

Possible orderings of the Ni and Al ions in the metal planes can also affect the stability of the compound. Several authors have reported observations of in-plane ordering of metal ions.<sup>2-6</sup> Ordering of ions was observed near the values of  $x$  equal to 1/4 and 1/3 that are in registry with the host geometry of a triangular lattice. However, as far as we know, there are no detailed experimental studies of the ordering as a function of composition  $x$ .

The ordering of metal ions in alloys is often considered within the framework of a lattice gas model in which only interactions between neighbors that are not separated by large distances are taken into account because of the relatively short screening length<sup>16-18</sup> caused by free electrons. It is generally accepted that in layered hydroxides the Coulomb interaction between positively charged metal planes, negatively charged hydroxide planes, and negatively charged anions  $[\text{CO}_3]^{2-}$  in the galleries is important. The screening length in layered hydroxides should be significantly larger than that in metal alloys, because dielectric screening caused

by water and other polar molecules is weaker than screening caused by free electrons. Thus a model that takes into account long-range Coulomb interaction and interaction between positive metal ions in the plane with negative hydroxides layers and negative anions in the galleries might be more suitable than a lattice-gas model to describe the ordering of metal ions in layered double hydroxides. The role of ordering due to Coulomb interactions has been discussed by Thompson.<sup>19</sup>

We have previously suggested a simple model to describe the ordering of metal ions in layered hydroxides.<sup>1</sup> In this model two kinds of positively charged metal ions occupy the sites of a triangular lattice. The lattice is immersed in a negatively charged background which represents the hydroxide layers and negative anions in the galleries. It was assumed that the background charge is the same at every site of the triangular lattice. Thus the total charge at every site is formed by the positive charge due to the metal ion and the negative background charge. The interaction potential between sites was assumed to be a long-range  $1/r$  Coulomb type.

In the previous work<sup>1</sup> the dependence of the ground-state energy of this model system on the concentration of Al was studied assuming a homogeneous concentration of metal ions in the plane. Equilibrium ordering configurations of ions that can occur at each concentration in the range  $0 \leq x \leq 1$  were calculated along with corresponding x-ray-diffraction patterns.

In this paper we suggest a different interpretation of the previous results. It will be shown that at some concentrations  $x$  the system is unstable with respect to phase separation into phases with concentrations  $x_1$  and  $x_2$  such that  $x_1 < x < x_2$ . We calculate the phase diagram of the system in the  $(T, x)$  plane using the grand canonical ensemble by introducing a chemical potential  $\mu$ . In the case of the layered hydroxides, the chemical potential under consideration is not related to the voltage on the electrodes and represents only a useful way to obtain the phase diagram.

The model is quite general and can be employed to describe ordering and first-order phase transitions in ionic systems with long range interactions. It may have some application to the ordering of intercalated Li ions in rechargeable Li batteries.<sup>19–21</sup> Predicted phase separations can lead to the staging at which homogenous planes with different concentrations of metal ions will form. In-plane long-range interaction in this case can be similar to that occurring in staged graphite intercalation compounds.<sup>22,23</sup>

The paper is organized as follows. In Sec. II we define our model. Then in Sec. III we discuss the details of the Monte Carlo (MC) method that was used to obtain the phase diagrams. Section IV describes an application of the method to the linear chain. Sections IV A and IV B are devoted to the case of finite ranges of interactions wherein an exact solution can be obtained using *transfer-matrix* techniques. The case of a linear chain with infinite-range Coulomb interaction in which the energies of equilibrium configurations can be calculated exactly using the *devil's staircase* method is discussed in Sec. IV C. Finally in Sec. V we study the case of the two-dimensional triangular lattice. Our results are summarized in the conclusion.

## II. MODEL

We consider a system composed of two types of positive ions which occupy the sites of some lattice. Every site of the lattice is occupied either by a *black* ion with charge  $Q_b$  or by a *white* ion with charge  $Q_w$ . The concentration of black ions is  $x$  and the concentration of white ions is  $1 - x$ . In addition to these two types of positive ions there is also a negative compensating uniform background charge  $q$ , at every site of the lattice, that ensures charge neutrality in the system. Hence at any site  $i$  we have a total charge equal to either  $\Delta_b = Q_b + q$  or  $\Delta_w = Q_w + q$ . The Hamiltonian of the system of charges can be written in terms of the pairwise interactions  $V_{ij}$  as

$$H = \sum_{i < j} V_{ij} \Delta_i \Delta_j. \quad (1)$$

For the Coulomb interaction,  $V_{ij} = 1/R_{ij}$ , where  $R_{ij}$  is the distance between sites  $i$  and  $j$ . In the following we will also consider the case of truncated Coulomb interaction for which there is interaction only between neighbors that are in some range.

The value of the background charge depends on the values of  $Q_b, Q_w$ , and on the concentrations of those ions. The average charge per site due to the positive ions is

$$\bar{q} = xQ_b + (1-x)Q_w. \quad (2)$$

The value of the charge that provides the uniform background with overall charge neutrality is then given by  $q = -\bar{q}$ . Thus  $\Delta_b = Q_b + q = (Q_b - Q_w)(1-x)$  and  $\Delta_w = Q_w + q = (Q_b - Q_w)(-x)$ . Introducing  $J_{ij} = V_{ij}(Q_b - Q_w)^2$  we rewrite Eq. (1) as

$$H = \sum_{i < j} J_{ij} (n_i - x)(n_j - x), \quad (3)$$

where  $n_i = 1$  if site  $i$  is occupied by a black ion and  $n_i = 0$  if site  $i$  is occupied by white ion. Thus the precise values of the positive charges do not change the general properties of the model. From Eq. (3) it follows that at a fixed concentration  $x$ ,

$$H = \sum_{i < j} J_{ij} n_i n_j - x^2 \sum_{i < j} J_{ij}. \quad (4)$$

Thus at a fixed concentration the model is essentially a lattice-gas model because in this case the second term in Eq. (4) is the same for all configurations of ions. This term is due to the neutralizing background and cancels the divergence of the energy associated with the Coulomb repulsion when the interactions are of infinite range.

It is easy to estimate the values of the constants  $J_{ij}$  if the lattice constant and charges  $Q_b$  and  $Q_w$  are known. For the aluminum-substituted layered nickel double hydroxide  $a = 3.032 \text{ \AA}$ ,<sup>7</sup>  $Q_b = 3e$  and  $Q_w = 2e$ . For the nearest neighbors we have

$$J = V_{nn}(Q_b - Q_w)^2 = \frac{e^2}{\epsilon a}. \quad (5)$$

Thus if we use a dielectric constant appropriate for water  $\epsilon \approx 80$ , then  $J \approx 60$  meV or about 500 K. Short-range screening, due to the presence of water and other ions, can effectively decrease the values of the  $J_{ij}$ .

In order to use the grand canonical ensemble to study the equilibrium properties of this system of charges, we add a chemical-potential term  $-\mu \sum_i n_i$  to the Hamiltonian. Now the concentration  $x$  can fluctuate and hence the background charge will also fluctuate. We write the grand canonical Hamiltonian as

$$H = \sum_{\langle ij \rangle} J_{ij} (n_i + q)(n_j + q) - \mu \sum_i n_i, \quad (6)$$

where  $q$  describes the uniform background charge which is adjusted to be equal to  $q = -\langle n_i \rangle = -x$ .

Our primary goal is to study the two-dimensional (2D) triangular lattice with infinite-range Coulomb interactions. However, we first consider the linear chain as an example to gain a better understanding of the model since there are exact analytical methods that can be used in two limiting cases: finite-range interactions can be studied exactly using transfer-matrix methods<sup>24</sup> and infinite-range Coulomb interactions can be described in terms of a devil's staircase formalism.<sup>16</sup> The study of the linear chain will give us insight into the precision of the numerical techniques that will be used for the triangular lattice with Coulomb interactions.

In the following sections we address these questions. What is the equilibrium structure of the charges for a given concentration of the ions? How does the equilibrium energy of the system depend on the concentration of the ions? How does the chemical potential depend on the average concentrations of the ions at different temperatures. Do phase transitions occur in the system and what is the phase diagram of the system at finite temperatures?

### III. MONTE CARLO METHOD FOR SIMULATIONS OF THE SYSTEM

We use a Metropolis algorithm<sup>25</sup> to accept or reject elementary moves that we perform on the charges to bring them into an equilibrium configuration. We use two different types of moves: *A* interchanges the positions of *black* and *white* ions in the lattice. *B* changes the *color* of the ion at a particular site.

The simulations can be carried out with either constant values of the concentration or with constant values of the chemical potential. In the case of simulations at a constant value of concentration only moves of type *A* were used. In the case of simulations at a constant value of the chemical potential both types of moves, *A* and *B*, were used. The *A* move does not change the value of the background charge since it does not change the concentration. The *B* move changes the concentration and thus the background charge has to be changed at every site in the lattice. In order to decide whether to accept or reject the move it is necessary to calculate the energy of the system before and after the move. We consider a lattice of size  $N$  in the case of the linear chain and  $N \times M$  for the triangular lattice. We apply standard periodic boundary conditions with respect to this *central zone*.

Thus the central zone occurs in the center of the bigger lattice surrounded by *surrounding zones*. In order to calculate the energy of the system we calculate the energy of interaction between all sites inside the central zone and the energy of interaction between the sites in the central zone with sites in all surrounding zones. Since the system is charge neutral, the contribution to the energy from surrounding zones that are far away from the central zone is much smaller than the contribution from surrounding zones that are close to the central zone. In fact, we found that if  $N$  and  $M$  are of the order of 10, then it is enough to consider the lattice of size  $5N \times 5M$  in order to calculate the energy with sufficient precision for almost all concentrations. In other parts of this paper we refer to the size of the central zone as the sample size, with the periodic boundary conditions described above.

The total energy of the system given by Eq. (3) can be separated into three parts which represent interactions between black-black, white-white, and black-white sites,

$$E = E_{bb} + E_{ww} + E_{bw}. \quad (7)$$

It follows from Eq. (3) that  $E_{bb}$  can be written as

$$E_{bb} = (1-x)^2 \sum_{i < j} J_{ij} n_i^b n_j^b. \quad (8)$$

In the sum above, the index  $i$  runs over all sites in the central zone and the index  $j$  over all sites in the central and surrounding zones ( $i \neq j$ ). The quantity  $n_i^b$  is unity if a black ion occupies site  $i$  and zero otherwise. Using the notation  $\sigma_{bb}(j) = \sum_i J_{ij} n_j^b$  Eq. (8) can be rewritten as

$$E_{bb} = (1-x)^2 \sum_i n_i^b \sigma_{bb}(i) = (1-x)^2 \sigma_{bb}. \quad (9)$$

In the same manner we can write  $E_{ww} = x^2 \sigma_{ww}$  and  $E_{bw} = 2x(1-x) \sigma_{bw}$ . Then the energy of the system per site can be written as

$$E = \frac{1}{2(N \times M)} [(1-x)^2 \sigma_{bb} + 2x(1-x) \sigma_{bw} + x^2 \sigma_{ww}], \quad (10)$$

where the first term in square brackets comes from the interaction between black-black sites, the second from black-white sites, and the third from white-white sites. It is easy to see from Eq. (10) that the equilibrium energy of the system is a symmetric function,  $E(x) = E(1-x)$ , with respect to  $x = 1/2$ . The ground states corresponding to concentrations  $x$  and  $1-x$  can be obtained from each other by changing all white sites into black sites and all black sites into white sites. In this case  $x \leftrightarrow 1-x$ ,  $\sigma_{bb} \leftrightarrow \sigma_{ww}$ , and  $\sigma_{bw} \leftrightarrow \sigma_{bw}$ , and it follows from Eq. (10) that the energy remains the same. In order to accept or reject the move we calculate the change in  $\Delta E - \mu \Delta x$ . For calculation of  $\Delta E$  it is necessary to take into account that if we turn a white site  $i$  into a black site, then charges at the sites corresponding to the site  $i$  but situated in the surrounding zones should be changed also. When an elementary move is performed, the values of  $\sigma_{bb}$ ,  $\sigma_{bw}$ , and  $\sigma_{ww}$  can be updated by calculating the sums  $\sigma_{bb}(i)$ ,  $\sigma_{bw}(i)$ ,

and  $\sigma_{ww}(i)$  for the particular site  $i$  that participate in the move. This significantly reduces the calculation time since it is not necessary to recalculate the energy of the whole lattice again after every move.

We say that one MC step was performed if we make one attempt to perform operation  $A$  or  $B$ . We say that one MC sweep was made if we make as many MC steps as there are sites in the sample. In simulations at a constant  $\mu$  we initially tried to vary the frequency with which operations  $A$  and  $B$  were performed, but we found that a 1:1 ratio was close to the optimum value. For every value of the concentration or the chemical potential, simulations start at a relatively high temperature  $T \approx J$ . If simulations are to be performed at constant  $x$  then in the initial configuration black and white ions in amounts corresponding to  $x$  are randomly distributed over the lattice sites. If simulations are to be performed at a constant value of  $\mu$ , the initial configuration is less important.

We used the following criteria to check the equilibration of the system at a given temperature. We let  $\bar{E}_2$  be the average value of the energy in the last ten MC sweeps and  $\bar{E}_1$  the average value of the energy in the previous ten MC sweeps. We let  $\sigma_{E_2}$  and  $\sigma_{E_1}$  be the average fluctuations of energy in those two cycles. If  $|\bar{E}_2 - \bar{E}_1| \leq \frac{1}{10} \min(\sigma_{E_1}, \sigma_{E_2})$  then we say that the system is sufficiently equilibrated in order to collect the data. If this condition is not fulfilled another ten MC sweeps are made until this condition is met, and so on.

After the equilibration, in order to obtain statistics, we calculated and stored the values of parameters of interest after every MC sweep. Their convergence to equilibrium values was verified by plotting them versus the number of the MC sweep. The number of required MC sweeps varied depending on the size of the system, type of interaction, and temperature. When the necessary data at a temperature  $T$  were collected, the temperature was decreased by a small amount  $\delta T$ . For smaller values of the temperature  $T$ , a smaller value of  $\delta T$  was used.

It will be shown below that first-order phase transitions occur in these systems. In other words ions on the lattice should separate into two parts with different concentrations of the black ions in each part. Parts with different concentrations of the black ions should also have different values of the background charge. But it is assumed in our model that the value of the background charge is the same everywhere. Thus the background in our simulations does not allow the systems to split into parts with different concentrations and thus does not allow the phase separation to be observed directly.

When we perform simulations at a constant value of average concentration  $\bar{x}$ , it is possible that we may choose some particular average value  $\bar{x}$  that cannot occur in a homogeneous system. The energy curve  $E(\bar{x})$  obtained in this case does not really give the dependence of energy on concentration, but rather shows when phase separation should occur. This is demonstrated explicitly in the next section using the linear chain as an example.

In simulations with a fixed value of the chemical potential the phase transitions are more pronounced. At high tempera-

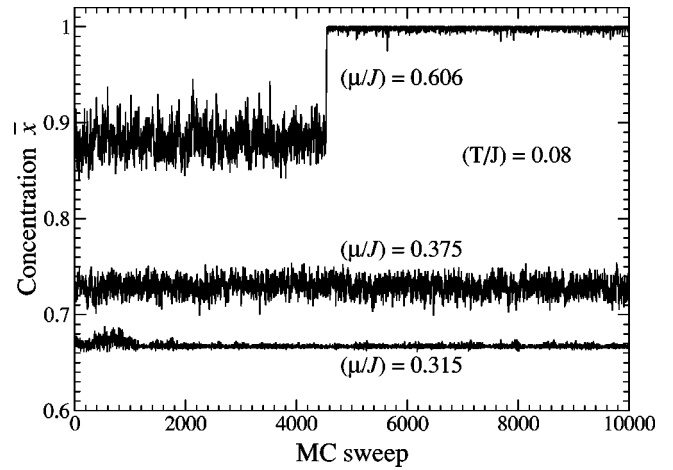


FIG. 1. Dependence of the concentration  $\bar{x}$  on MC sweeps at fixed values of the chemical potential  $\mu$  at temperature  $(T/J) = 0.08$  for the triangular lattice with  $30 \times 30$  sites in the sample. The values of  $\mu$  are shown near their corresponding curves.

tures  $(T/J) \geq 1$ , changes in the chemical potential lead to smooth changes in average concentration  $\bar{x}$ . However, at low temperatures  $(T/J) \ll 1$ , there are discontinuities in the  $\bar{x}(\mu)$  curve. We assume that the borders of the discontinuity region are the borders of the phase-separation region.

The situation at intermediate temperatures is more complicated. As an example, Fig. 1 shows the concentration as a function of the number of MC sweeps for a  $30 \times 30$  triangular lattice for three values of  $\mu$  at  $(T/J) = 0.08$ . The sharp jump in concentration from  $\bar{x} \approx 0.88$  to  $\bar{x} = 1$  that occurs at  $\mu/J = 0.606$  shows that both concentrations  $\bar{x} \approx 0.88$  and  $\bar{x} = 1$  lead to the same minimum value of Helmholtz free energy and thus are stable. Homogeneous equilibrium configurations in the range of concentrations  $0.88 < \bar{x} < 1$  have higher values of the Helmholtz free energy and thus are unstable with respect to phase separation into two parts with concentrations  $\bar{x} = 0.88$  and  $\bar{x} = 1$ .

Figure 2 shows the histogram of the distribution of concentrations corresponding to those in Fig. 1. Peak positions give us the values of average concentrations. For some particular values of  $\mu$  the system migrates between two significantly different concentrations, as, for example, for  $\mu = 0.606$ . We assume in this case that there is phase separation, and relative areas under two peaks give us the relative sizes of the two phases. Thus the appearance or disappearance of a peak tells us about the appearance or disappearance of a phase. We use the positions of the peaks when they appear or disappear as the borders of the two phase coexistence regions.

At low temperatures  $(T/J) \ll 1$  our MC procedure becomes less effective and the system can become frozen in some configurations. One of the reasons for this is the local character of the moves  $A$  and  $B$  that we use to search for a new configurations, e.g., every MC move involves only one or two sites. To study the properties of the system at very low temperatures and critical behavior of the model (when simu-

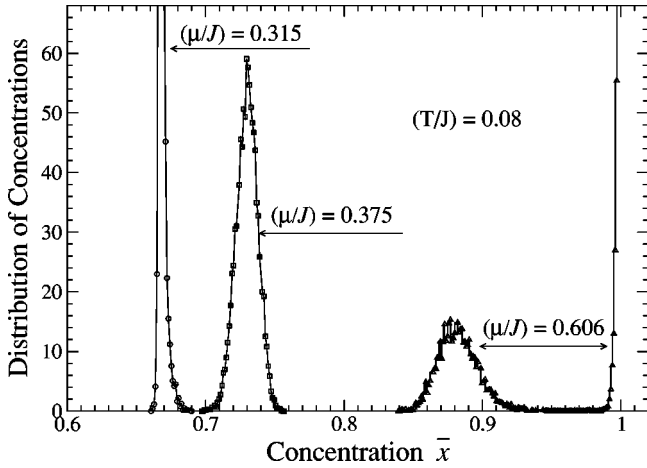


FIG. 2. Histograms that show distributions of concentrations for the curves from Fig. 1. Data were collected over 10 000 MC sweeps. The sharp peak corresponding to  $(\mu/J)=0.315$  has a height 4000. The peak corresponding to  $(\mu/J)=0.606$  has a height 1700.

lations of the large systems are required) it might be useful to implement other simulation methods,<sup>26</sup> but that is not the objective of the present work.

#### IV. LINEAR CHAIN

There are two exact analytical methods to study the model in the one-dimensional case of the linear chain. In particular, if the Coulomb interaction is truncated at some distance then a transfer-matrix<sup>24</sup> technique can be applied to calculate the free energy as a function of chemical potential and temperature. Then the dependence  $x(\mu, T)$  can be studied and the phase diagram can be obtained.

In the case of the infinite-range Coulomb interaction at  $T=0$ , a devil's staircase<sup>16</sup> formalism can be used to predict the equilibrium structure for any concentration and calculate the ground state energy of the system. In both cases exact results will be compared with the results of simulations to establish the precision of the numerical methods.

##### A. Nearest-neighbors interaction

If we restrict the range of interaction to nearest neighbors only, the Hamiltonian becomes

$$H = J \sum_i (n_i + q)(n_{i+1} + q) - \mu \sum_i n_i. \quad (11)$$

Initially we assume that  $q$  is a constant and is not connected with concentration. Then the grand partition function  $\mathcal{Z}_N$  for a cyclic chain of  $N$  sites can be expressed in terms of the largest eigenvalue of the  $2 \times 2$  transfer matrix as  $\mathcal{Z}_N = \lambda_{max}^N$  with

$$\lambda_{max} = \frac{e^{-\beta J q^2}}{2} \left[ 1 + \gamma + \sqrt{(\gamma - 1)^2 + 4\gamma e^{\beta J}} \right], \quad (12)$$

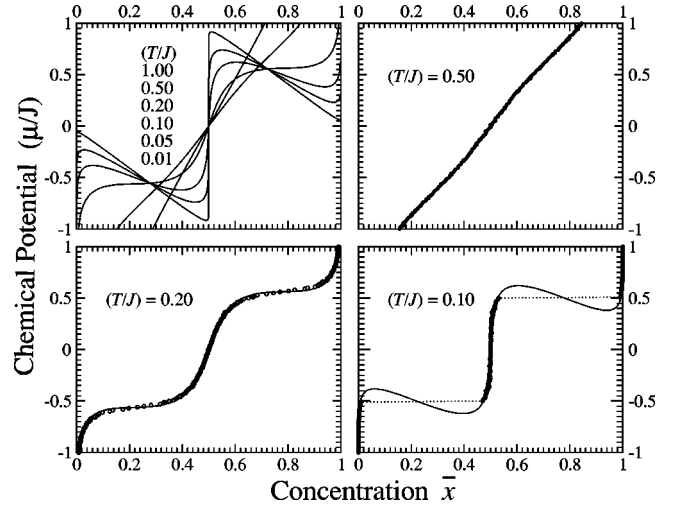


FIG. 3. Dependence of the chemical potential  $\mu$  on the average concentration  $\bar{x}$  for the case of a linear chain with interaction limited to nearest neighbors only. The plateaus seen in simulations for  $(T/J)=0.10$  correspond to the regions of phase separation.

where  $\gamma = e^{\beta(\mu + 2Jq - J)}$  and  $\beta = 1/(k_B T)$ . The grand potential per site is given by  $\Omega = -k_B T \ln[\lambda_{max}]$ . Using the fact that  $\bar{x} = \langle n_i \rangle = \partial \Omega / \partial \mu$ , we can find  $\bar{x}$  as a function of the independent variables  $T$  and  $\mu$ . The resulting expression can then be inverted using the charge neutrality requirement,  $q = -\bar{x}$ , to obtain  $\mu$  in terms of  $\bar{x}$  and  $T$  with the following result:

$$\mu = J - 2J\bar{x} + \frac{2}{\beta} \sinh^{-1} \left[ \frac{(\bar{x} - 1/2)e^{\beta J/2}}{\sqrt{\bar{x}(1 - \bar{x})}} \right]. \quad (13)$$

Figure 3 shows the transfer-matrix predictions for the  $\mu$  versus  $\bar{x}$  curves for various values of  $T/J$  and also the results of numerical simulations. The upper left frame shows the results of the transfer-matrix calculations at various temperatures.

Note that  $\mu = 0$  corresponds to  $\bar{x} = 1/2$ . At high temperatures,  $\mu$  is a monotonically increasing function of  $\bar{x}$  but at low temperatures,  $\mu$  has regions in which the slope is negative. This behavior is thermodynamically unstable and indicates that phase separation occurs. The upper right frame shows transfer-matrix predictions and the results of simulations at  $(T/J)=0.50$ . Simulation points lie on top of the exact curve. The lower left frame shows the results at temperature  $(T/J)=0.20$  which is just above the maximum temperature for which phase separation occurs. The regions with a low density of simulation points indicate the appearance of the regions of phase separation that occur at lower temperatures. The concentration  $\bar{x}$  in this region is the average over the two peaks that occurs at the intermediate temperatures as shown in Fig. 1 and Fig. 2. The lower right frame at  $(T/J)=0.10$  clearly shows the sharp jumps in concentration that occur at low temperatures.

In the simulations, phase separation manifests itself as a discontinuity in the dependence  $\bar{x}(\mu)$ . In contrast, a second-

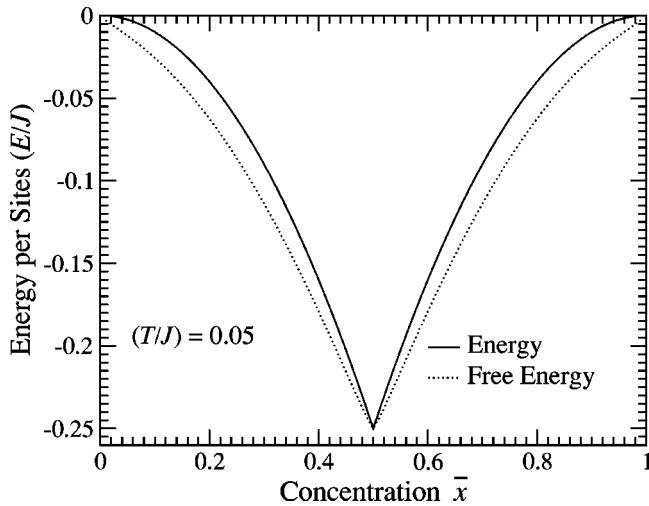


FIG. 4. Energy and Helmholtz free energy as functions of the average concentration  $\bar{x}$  at temperature  $(T/J)=0.05$  for a linear chain with interaction limited to nearest neighbors only.

order transition would correspond to  $\mu$  increasing monotonically with a discontinuity in slope.

The first-order transition can also be seen in plots of the grand potential per site,  $\Omega$ , versus chemical potential. Loops corresponding to the unstable branches appear at low temperatures. However, we find it more convenient to plot the Helmholtz free energy per site,  $F = \Omega + \bar{x}\mu$ , or the internal energy per site,  $E$ , as a function of the concentration  $\bar{x}$ .

A finite temperature phase transition is not expected in one dimension for finite-range interactions. However, the presence of the background charge effectively makes this an infinite-range problem and produces a first-order phase transition at a finite temperature. This behavior is similar to that in the van der Waals theory of liquids where long-range attractive interactions lead to condensation phenomena.

Figure 4 shows both energy  $E$  and Helmholtz free energy  $F = E - TS$  as functions of  $\bar{x}$  at  $(T/J)=0.05$ . The difference between these two curves is due to the entropy of the system. The difference between these two curves is significant, because the entropy plays an important role even at quite low temperatures.

Since  $\bar{x}$  is the independent coordinate, we apply the double tangent rule to the Helmholtz free energy  $F$  (or to the energy curve at  $T=0$ ) to determine the equilibrium concentration. The slope of the tangent line gives the value of the chemical potential  $\mu$ . This predicts that at  $T=0$  the system will separate into two phases with concentrations 0 and 1/2 if  $\bar{x}$  is between those two concentrations. If  $1/2 < \bar{x} < 1$  then the system will separate into two phases with concentrations 1/2 and 1. Hence a plot of  $\mu$  versus  $\bar{x}$  should display flat horizontal sections at values of  $\mu$  corresponding to the slopes of the double tangent lines. This process is equivalent to a Maxwell construction applied to the regions in Fig. 3 at which the  $\mu(x)$  dependence has a negative slope.

If in MC simulations we are trying to produce the  $E(\bar{x})$  curve and we fix the concentration at a particular value that cannot exist homogeneously across the system, then we cre-

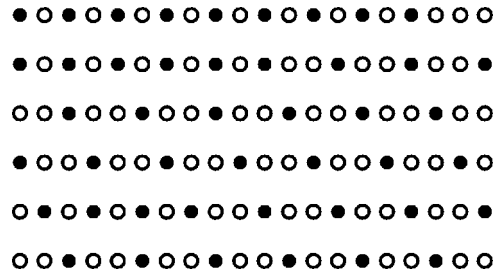


FIG. 5. The linear chain sample of 120 sites with interactions up to fifth neighbors included at  $\bar{x}=3/8=0.375$  and temperature  $(T/J)=0.01$ . The second row from the top is the continuation of the first row, and so on. The picture illustrates the tendency of the system to phase separate: In the top row  $x \approx 1/2$ , while in the bottom row  $x \approx 1/3$ . Separation cannot really occur due to the same background charge at every site of the chain that corresponds to  $\bar{x} = 3/8$ .

ate an internal stress in the system: the ions tend to separate into two phases but the background charge, through Coulomb interaction, does not allow this phase separation since it is constrained to be uniform. This stress should effectively increase the value of the energy  $E(\bar{x})$  in the simulations. It is possible sometimes to see in structures obtained from simulations the tendency to phase separate. In Fig. 5 one can clearly see this tendency for the phase separation: The average concentration in the top row is 1/2 while the average concentration in the bottom row is 1/3.

Figure 6 shows the phase diagram in the temperature–concentration plane. The solid curve is the transition temperature  $T_c$ . This curve was obtained using the equal area rule applied to the  $\mu$  versus  $\bar{x}$  curves (see Fig. 3) obtained from Eq. (13). The dashed curve is the spinodal which corresponds to the locus of points for which  $(\partial\mu/\partial\bar{x})=0$ . The spinodal is only shown in the region  $x < 1/2$  but it is sym-

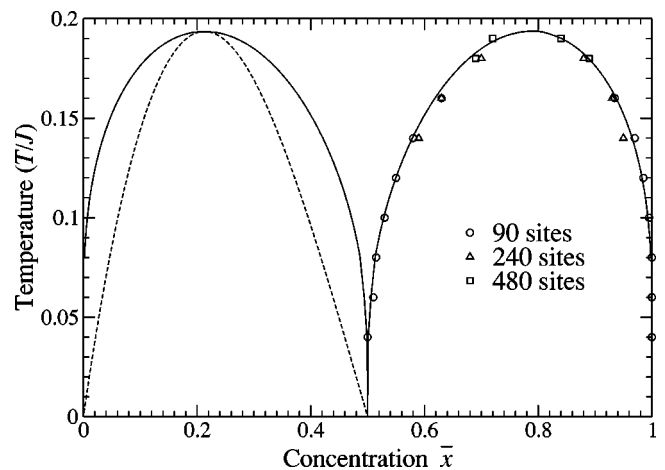


FIG. 6. Phase diagram for a linear chain with nearest-neighbor interactions. The solid lines indicate the borders of the phase-separation regions. The dashed curve shown for  $x < 1/2$  only is the spinodal curve. Both curves were obtained with the transfer-matrix method. The points on the right show the results of the simulations performed on lattices with different sample sizes.

metric with respect to  $x=1/2$ . The regions between solid and dashed curves correspond to the regions of metastability.

In order to obtain the phase diagram in MC simulations at low temperatures ( $T/J \leq 0.12$ ) we refer back to Fig. 3. The plateaus in the  $\mu(x)$  dependence give us the concentrations for which phase separation occurs. In other words, any concentration on any plateau should split into the two concentrations on the edges of the same plateau. Thus the edges of the plateaus give us the borders of the two phase coexistence regions and the phase diagram of the system. This approach gives good agreement with exact results at low temperatures but fails at intermediate temperatures when fluctuations in the concentration are big or when the system migrates between two different concentrations. To obtain the phase diagram at intermediate temperatures  $0.14 \leq (T/J) \leq 0.20$  we used the observations and interpretation that we discussed in Sec. III. In Fig. 6 data for the sample with 90 sites were obtained from the borders of the jumps in  $x(\mu)$  curves shown in Fig. 3. The remaining points are obtained from the distribution of concentrations at different  $T$  and  $\mu$  using larger sample sizes. The peaks in the distributions of concentrations for the sample with 480 sites are narrower than those with 240 sites, as expected. The full width at half maximum for the peaks at temperatures  $(T/J) \approx 0.14$  is about 0.05 and at temperature  $(T/J) \approx 0.18$  about 0.1. Thus at temperature  $(T/J) \approx 0.18$  peaks corresponding to two different concentrations overlap.

The good agreement between the exact phase diagram and the one obtained from simulations indicates that our interpretation of the histogram of the concentration frequencies is correct. It also indicates the precision of our technique.

### B. Finite range of interaction

The Hamiltonian of the model at fixed concentration  $x$  is given by Eq. (3). In the case of nearest-neighbor interaction  $J_1$  and second-neighbor interaction  $J_2$  only, the ground-state energy can be obtained directly using the following reasoning: for concentrations in the range  $0 < x < 1/3$ , the background charges (white charges) contribute an amount  $-(J_1 + J_2)x^2$  to the energy per site from the last term in Eq. (4). The black charges can be placed on every third site so as to avoid the repulsion in the first term. However, in the concentration range  $1/3 < x < 1/2$  the repulsive interactions contribute an additional amount  $(J_1 + J_2)(x - 1/3)$  to the energy. The energy in the range  $1/2 < x < 1$  is obtained using the symmetry property  $E(x) = E(1-x)$ . Similar reasoning can be used for larger ranges of the interactions but the expressions become more complicated.

Figure 7 shows the ground-state energies as a function of concentration  $\bar{x}$  at  $T=0$ , for finite-range interactions  $J_n = J/n$ , where the truncation is after  $n=1, 2, 3, 4, 5$ , and 6. The solid curves were obtained using the arguments described above and were verified using the numerical transfer-matrix method results at very low temperatures. The MC simulations were performed on lattice samples with 90 and 180 sites and periodic boundary conditions.

Panel 2 in Fig. 7 shows the energy curve for the interaction between nearest and second-nearest neighbors only. It is

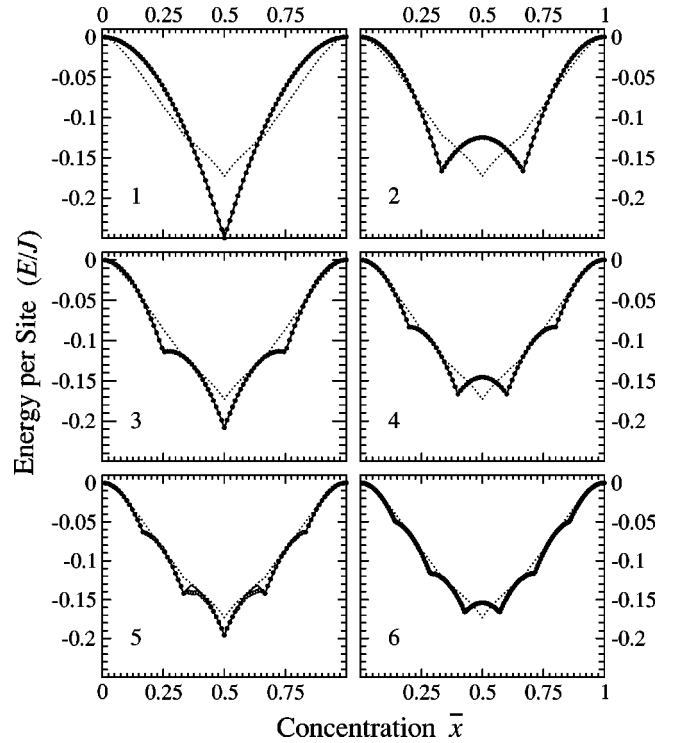


FIG. 7. Dependence of the energy per site on concentration, at very low temperatures, for the linear chain with interaction extending up to first, second, third, fourth, fifth, and sixth neighbors. Points from simulations are plotted on top of the exact solid curves obtained with the transfer-matrix technique. The dotted curve shows the limiting case of infinite-range Coulomb interaction.

easy to see that for  $\bar{x}=1/2$  it is energetically favorable for the system to split into two parts with different average concentrations  $\bar{x}_1=1/3$  and  $\bar{x}_2=2/3$ .

If we apply the double tangent construction to the  $E(\bar{x})$  curves in Fig. 7, corresponding to interactions with larger range, we find additional transitions compared to the nearest-neighbor case. For interaction up to second neighbors we have first-order transitions from  $x=0$  to  $x=1/3$ ,  $x=1/3$  to  $x=2/3$ , and  $x=2/3$  to  $x=1$ . For neighbors up to the third included, there are four transitions involving  $x=0$ ,  $1/4$ ,  $1/2$ ,  $3/4$ , and 1.

As the range of interaction increases there is an increasing amount of structure in the energy curves but the double tangent construction does not always lead to an increasing number of transitions. It is shown in the next section that in the limit of Coulomb interactions, the energy curve approaches a form which predicts only four transitions involving the values  $x=0$ ,  $1/3$ ,  $1/2$ ,  $2/3$ , and 1.

Phase separations predicted from the energy curves cannot occur in our MC simulations because this phase separation requires two different values of the background charge, while in our simulations background charge is constrained to have the same value at every site. However, if concentrations of the two parts are close to each other then the tendency to phase separate can be seen even if the value of the background charge is the same everywhere as shown in Fig. 5. This behavior can also be seen on the fifth panel of Fig. 7

that shows a disagreement between the exact curve and results of simulations for the case of interaction up to fifth neighbors. There is a region between  $0.325 \leq \bar{x} \leq 0.425$  in which simulation points seem to follow a horizontal line while the exact curve has a peak in this region. We believe that the origin for this behavior is the tendency to phase separate as described above. Thus every simulated point in this region is a weighted average of two concentrations that correspond to the edges of this horizontal region. The weight is proportional to the fraction of the whole sample.

In order to apply the transfer-matrix method to the case with range of interaction  $n \geq 2$  neighbors, we can group the sites into consecutive blocks of length  $n$  and the interactions are then only between nearest blocks. The transfer-matrix formalism can be used again, but the Hamiltonian given by Eq. (6) leads to the transfer matrix of size  $2^n \times 2^n$  and it is difficult or impossible to solve the problem analytically. However, it is possible to calculate the largest eigenvalue of the transfer matrix numerically and obtain the thermodynamic properties. We have used this method to study the energy, Helmholtz free energy, and chemical potential as a function of concentration  $\bar{x}$ . Our results are in agreement with the predictions made from the energy curves, shown in Fig. 7.

### C. Infinite-range Coulomb interaction

If  $J_{ij}$  correspond to the bare Coulomb interaction, the interactions satisfy the positivity and convexity condition<sup>16</sup> which allows the ground state to be found for any rational value of  $\bar{x}$ . If  $\bar{x} = 1/n$  where  $n$  is an integer, then the black charges are equally spaced along the chain at a distance of  $n$  neighbors apart and form the one-dimensional analog of the Wigner lattice.<sup>27</sup> In the more general case in which  $\bar{x} = p/q$  is the ratio of two integers, the ground-state configuration is periodic with period  $q$  and has  $p$  black charges in each cell. If there is a black charge at site 0 then black charges are at the sites with numbers  $[nq/p] = [n/\bar{x}]$  where  $n$  is any integer and  $[A]$  denotes the integer part of  $A$ . Since the structure is known for any rational value of  $x$  the ground-state energy can be calculated using the same techniques that were used to calculate energies in MC simulations. But since in this case it is not necessary to run a relaxation procedure, much larger samples can be considered.

Figure 8 shows the ground-state energy as a function of  $x$  for the Coulomb potential obtained using both the exact ground-state configurations and our simulation technique. The value of the energy at  $x = 1/2$  corresponds to alternating black and white charges and is equal to  $-(\ln 2)/4$ . For smaller values of  $x = 1/n$  corresponding to period  $n$  Wigner lattices of equally spaced black charges, the energy per site is given by  $E = x^2 \ln x$ . For values of  $x$  between these values the energy is slightly larger than if we use the same formula for all  $x$ . The energy curve has a sequence of cusps located at all rational values of  $x$  (devil's staircase).

Since at  $T=0$ , the chemical potential is given by  $\mu = \partial E / \partial x$ , we predict that at zero temperature  $\mu$  versus  $\bar{x}$  will display a series of jumps as shown in Fig. 9. The double

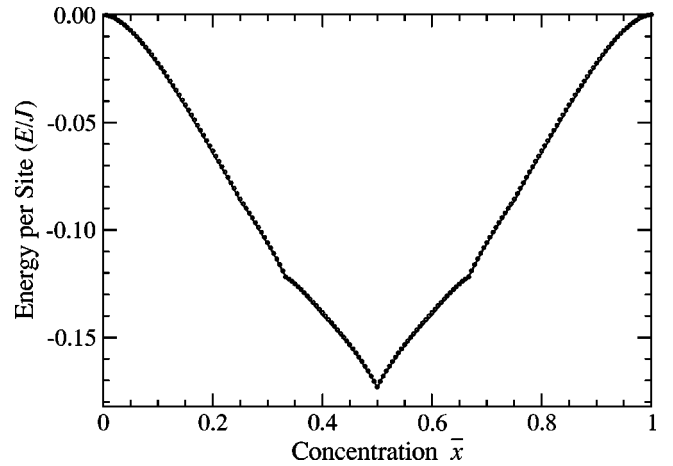


FIG. 8. Energy per site as a function of concentration  $\bar{x}$  for a linear chain with Coulomb interactions. The solid curve was obtained by knowing equilibrium structures predicted with the devil's staircase formalism on the lattice sample with 1000 sites. Circles show the results of the MC simulations at low temperature for samples with 180 sites.

tangent rule applied to the energy curve predicts phase separations for some values of  $\bar{x}$ . For  $0 < x < 1/3$ , the system should separate into phases with  $x=0$  and  $x=1/3$  whereas, for  $1/3 < x < 1/2$ , it should separate into phases with  $x=1/3$  and  $x=1/2$ .

Phase separation is a result of the second term in Eq. (4), which is entirely due to the background. It corresponds to a long-range attractive interaction. In the absence of the background, the model would not display phase separation and the chemical potential versus concentration curve would be a

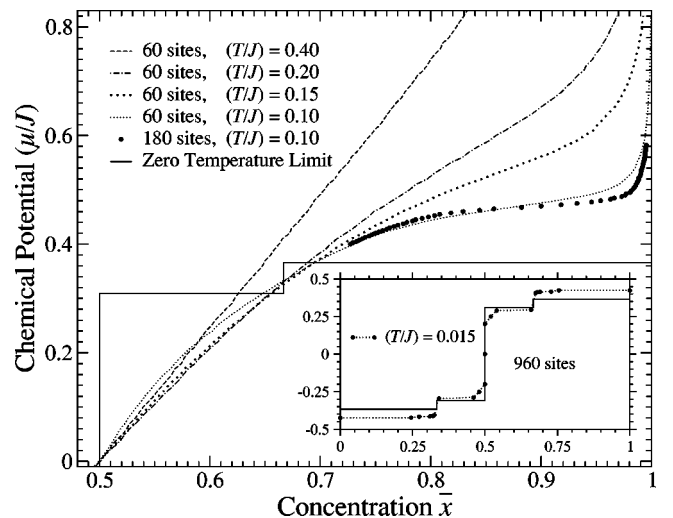


FIG. 9. Dependence of the chemical potential  $\mu$  on concentration  $\bar{x}$  for the linear chain with Coulomb interaction in the region  $\bar{x} > 1/2$ . The solid line shows the limit of zero temperature obtained from the energy curve in Fig. 8. The inset shows the results from the lattice sample with 960 sites at very low temperatures in the whole range  $0 < \bar{x} < 1$ .

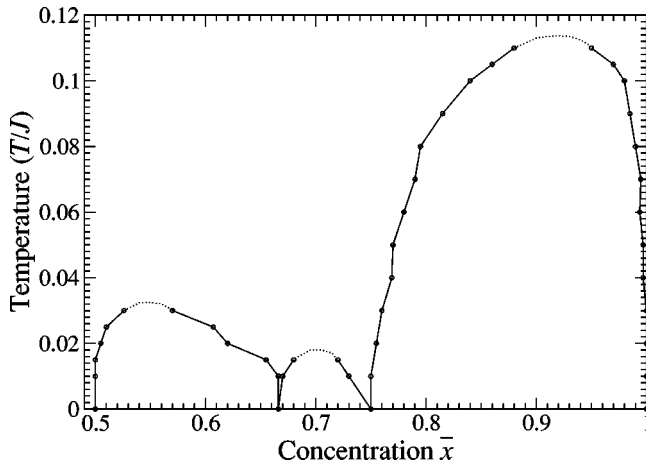


FIG. 10. Phase diagram for the linear chain with Coulomb interactions in the region  $x > 1/2$  obtained from MC simulations.

devil's staircase with an infinite number of jumps corresponding to the rational values of  $x$ .

The devil's staircase formalism can be used to obtain the  $E(\bar{x})$  curve at zero temperature and thus predict  $\mu(x)$  dependence at zero temperature. In order to obtain the  $\mu(x)$  dependence at nonzero temperature we used MC simulations. The  $\mu(x)$  curves at several temperatures obtained from MC simulations are shown in Fig. 9. Simulations were performed on samples with 60, 90, 120, 180, and 960 sites. The role of size effects can be seen for the curve  $(T/J) = 0.10$  for which the results from the samples with 60 and 180 sites are shown. For higher temperatures the differences are less significant. We found that up to very low temperatures there are almost no differences between the results on samples with 120 and 180 sites.

The inset in Fig. 9 shows a rather large difference between the predictions for  $\mu(x)$  from the devil's staircase formalism and from the results of simulations at low temperatures. There can be several reasons for this disagreement. One reason, discussed earlier, is that simulations at low temperatures may not be reliable since the system can become frozen in some local minima that it cannot leave due to the large transition barrier associated with the local character of moves  $A$  and  $B$ . On the other hand the entropy contribution can make the "cusp" at  $x = 1/3$  and  $x = 2/3$  in the  $E(\bar{x})$  dependence more "rounded" and this can lead to an extended range of chemical potential near concentrations  $x = 1/3$  and  $x = 2/3$  on the  $\mu(x)$  curve.

In order to obtain the phase diagram shown in Fig. 10 we used the MC technique already discussed above. As expected, the size of the plateaus corresponding to the regions of phase separation decreases as the temperature increases and the concentrations of both phases become the same at the critical temperature. Only half of the phase diagram is shown since it is symmetric with respect to  $x = 1/2$ . At temperatures  $0.04 \leq (T/J) \leq 0.08$  the data were obtained using a sample with 480 sites. At other temperatures the data were obtained using a sample with 960 sites. There are three distinct regions of phase separation that correspond to the following transitions in concentration at zero temperature:  $1/2$

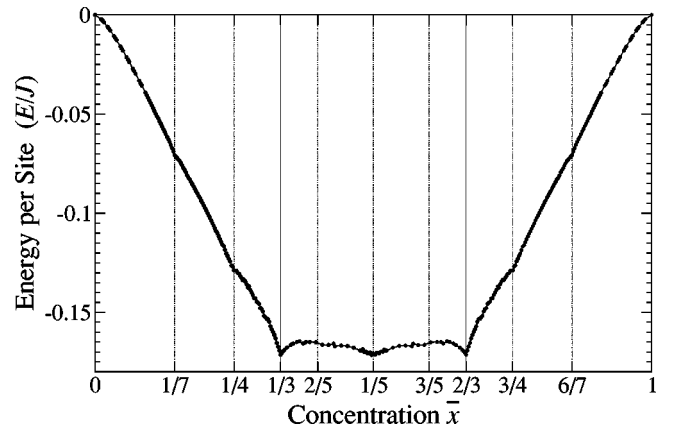


FIG. 11. Energy per site as a function of concentration  $\bar{x}$  for the triangular lattice with Coulomb interactions. The solid curve connects the points obtained by simulations in previous work (Ref. 1). Dashed vertical lines give the position of concentrations that are stable in MC simulations at very low temperatures.

$\rightarrow 2/3$  with critical temperature  $(T/J) \approx 0.03$ ,  $2/3 \rightarrow 3/4$  with critical temperature  $(T/J) \approx 0.0175$ , and  $3/4 \rightarrow 1$  with critical temperature  $(T/J) \approx 0.11$ .

## V. TRIANGULAR LATTICE

The Hamiltonian for the triangular lattice with Coulomb interaction is given by Eq. (6) to be

$$H = \sum_{\langle ij \rangle} J_{ij}(n_i + q)(n_j + q) - \mu \sum_i n_i. \quad (14)$$

The details of model and simulation techniques were described in Secs. II and III. In the 2D case with long-range interaction we used MC simulations as the main method to study the system. Different sample sizes were used in the previous study<sup>1</sup> in order to obtain  $E(\bar{x})$  dependence as shown in Fig. 11.

For the triangular lattice there are multiple "cusps" in the  $E(\bar{x})$  curve that are similar to the devil's staircase behavior in the case of the one-dimensional chain. In the region  $1/2 \leq \bar{x} \leq 1$  significant cusps in the  $E(\bar{x})$  curve occur at concentrations  $1/2$ ,  $2/3$ ,  $3/5$ ,  $3/4$ , and  $6/7$ .

Ground-state configurations for  $x = 1/2$ ,  $3/5$ ,  $2/3$ , and  $3/4$  are shown in Fig. 12. Ion distributions obtained on the  $30 \times 30$  sample with MC simulations at three different values of  $\mu$  at  $(T/J) = 0.01$  are shown in Fig. 13. In the ground state at  $x = 6/7$  white sites should form a triangular Wigner lattice with the spacing  $a\sqrt{7}$  between ions.<sup>1</sup>

For values of  $x = 1/(m^2 + n^2 + mn) \leq 1/3$  or  $1 - x \geq 2/3$  where  $m$  and  $n$  are integers, the ground-state configurations are triangular Wigner crystals<sup>27,28</sup> and the ground-state energy can be calculated exactly using the numerical formalism of Bonsall and Maradudin.<sup>29</sup> For these triangular Wigner crystal structures the energy is given exactly<sup>30</sup> by  $E(x) = -2.10671262(x^{3/2} - x^2)$ . Between  $x = 1/2$  and  $x = 2/3$ , the ground-state configurations have a rectangular rather than triangular geometry. Regular rectangular structures can be

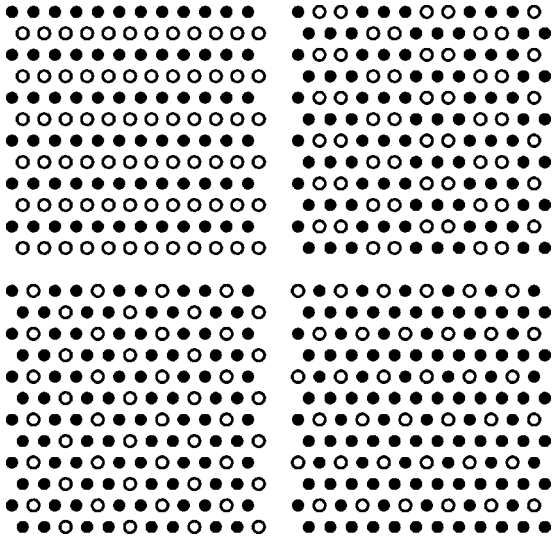


FIG. 12. Ground-state configurations for the triangular lattice with Coulomb interaction for  $x=1/2$ ,  $3/5$ ,  $2/3$ , and  $3/4$ .

formed at concentrations  $x=l/[2(l+1)]$ , where  $l$  is any integer.<sup>1</sup> Thus  $l=4$  corresponds to  $x=2/5$  and is the same structure as for  $x=3/5$  with the interchange of black and white sites. The same numerical method<sup>29</sup> can be used again to obtain  $E(3/5)=-0.1709803$  and  $E(1/2)=-0.1755589$ .

The first row of Table I shows the values of the energies obtained from simulations at  $(T/J)=0.002$  with sample sizes  $\approx 18 \times 18$ . For every concentration, the sample size was chosen to be commensurate with a particular concentration. The second row shows the results of simulations from the lattice samples of size  $\approx 30 \times 30$ . The third row of the table shows the exact values of the energies obtained with the method of Bonsall and Maradudin.

The major difference between the simulated and the exact values arises because our simulation method cannot relax the system to the exact ground-state configurations for concentrations  $1/2$ ,  $3/5$ ,  $3/4$ , and  $6/7$ . On the other hand it is easy to obtain the ground-state configuration for  $x=2/3$  and the agreement between the simulated and the exact values of the energy is much better in this case.

Double tangent construction applied to the energy curve in Fig. 11 shows that only concentrations  $0$ ,  $1/4$ ,  $1/3$ ,  $1/2$ ,  $2/3$ ,  $3/4$ , and  $1$  are stable with respect to the phase separation at zero temperature. Thus at zero temperature the system is always a mixture of parts with these concentrations. For ex-

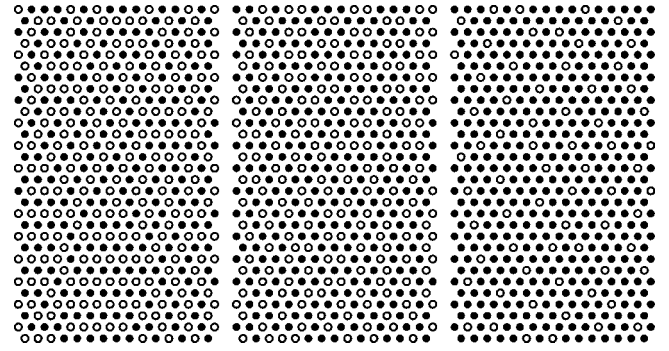


FIG. 13. Lattice structures obtained from simulations at three different values of  $\mu$  at  $(T/J)=0.01$ . Concentrations of black ions are close to  $x=1/2=0.5$ ,  $x=3/5=0.6$ , and  $x=6/7 \approx 0.857$  for the pictures from left to right.

ample, if  $\bar{x}$  is between  $0$  and  $1/4$  then the system should split into two homogeneous parts with  $x=0$  in one part and  $x=1/4$  in another.

The slope of the double tangent lines gives the values of chemical potential at which the transition from one concentration to another should occur. In the region  $x > 1/2$  we have  $(\mu/J)_{1/2 \rightarrow 2/3}=0.0003$ ,  $(\mu/J)_{2/3 \rightarrow 3/4}=0.5087$ , and  $(\mu/J)_{3/4 \rightarrow 1}=0.5159$ . The corresponding dependence  $\mu(x)$  at zero temperature is shown in Fig. 14 as the dotted curve.

Direct simulations of the  $\mu(x)$  curve were performed on lattices of different sample sizes  $9 \times 9$ ,  $18 \times 18$ ,  $18 \times 20$ ,  $24 \times 24$ , and  $30 \times 30$ . Some results are shown in Fig. 14. Crosses for the sample size  $18 \times 18$  show that there is no large difference with the results obtained on the sample of size  $9 \times 9$  at  $(T/J)=0.10$ . For higher temperatures the difference is even less significant.

When we consider long-range interactions in two dimensions, the amount of time needed to calculate the energies before and after the MC step increases quickly with the size of the system. In order to save time we tried to perform calculations on smaller samples when possible. Thus at high temperatures, we performed simulations on small  $9 \times 9$  samples. Every point is the result of averaging over 20 000 MC sweeps. Even at  $(T/J)=0.05$  there is almost no difference between the results of simulations on the lattices  $18 \times 18$  and  $30 \times 30$ . However, at very low temperatures, there are some structures that can be observed only on large samples. For example, at a temperature  $(T/J) \leq 0.03$  we can clearly see concentrations  $3/5$  and  $6/7$  on the  $30 \times 30$  sample, but we cannot see these concentrations on the  $18 \times 18$  sample and they are not pronounced in the case of the  $24 \times 24$  sample.

TABLE I. Comparison of energies at special concentrations obtained in simulations on lattices with sample sizes  $18 \times 18$  in the first row and  $x \approx 30 \times 30$  in the second row and exact values calculated with method of Bonsall and Maradudin in the third row (Ref. 29).

$\bar{x}$	1/2	3/5	2/3	3/4	6/7
$E_{sim}(18 \times 18)$	-0.17056	-0.16534	-0.16953	-0.12450	-0.06794
$E_{sim}(30 \times 30)$	-0.16964	-0.16456	-0.17070	-0.12671	-0.06807
$E_{exact}$	-0.17556	-0.17098	-0.17136	-0.13167	-0.07076

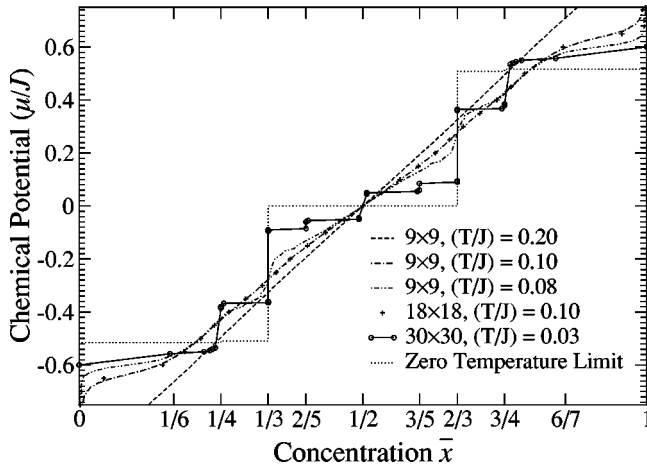


FIG. 14. Dependence of chemical potential  $\mu$  on concentration  $\bar{x}$  for the triangular lattice with Coulomb interaction. For the cases of temperatures  $(T/J)=0.2$  and  $(T/J)=0.1$  the size of the sample was  $9 \times 9$  and no points are shown since their density is high.

At low temperatures ( $T \approx 0.01$ ) there is a significant difference between the direct simulations of  $\mu(x)$  dependence and the predictions from the  $E(x)$  curve. In the simulations, the ranges of stability (with respect to the change in chemical potential) at concentrations  $x = 1/4$ ,  $3/4$ , and  $1/2$  are much larger than they should be according to predictions from the energy curve, while at concentrations  $x = 1/3$  and  $2/3$  the ranges of stability are smaller. In simulations we also see stable concentrations  $2/5$  and  $3/5$  that should not appear according to the energy curve. Several effects can lead to this disagreement.

First of all, the difference between the energy and the free-energy curves can be significant even at very low temperatures. This difference can lead to higher stabilities of some concentrations. Moreover, some concentrations that should not appear, as follows from the energy curve, can appear due to entropic contributions to the free energy. For example, configurations at  $x = 1/3$  and  $x = 2/3$  are highly ordered and have relatively small entropy. The concentrations between  $x = 1/3$  and  $x = 2/3$  are highly disordered (large entropy) and have approximately the same energy as energy of the system at concentrations  $1/3$  and  $2/3$ . Thus one can expect that concentrations  $1/3$  and  $2/3$  will have a smaller range of stability in  $\mu$ , while concentration  $1/2$  will be more stable than follows from energy curve predictions. This is in agreement with Fig. 14. This feature can also lead to the appearance of some configurations with  $1/3 < x < 1/2$  and  $1/2 < x < 2/3$ , for example,  $x = 2/5$  and  $x = 3/5$ . It also explains why we see these concentrations on larger samples and not on smaller samples.

Another reason can be in the way simulations were performed at a constant value of the concentration. For example, if the system has an average concentration  $1/2 < \bar{x} < 2/3$  then it should separate into two parts with concentrations  $x = 1/2$  and  $x = 2/3$ . But since at every site the background charge is the same, the system cannot separate. This tendency of the system to phase separate, which cannot occur, creates internal stress and effectively increases the energies of interme-

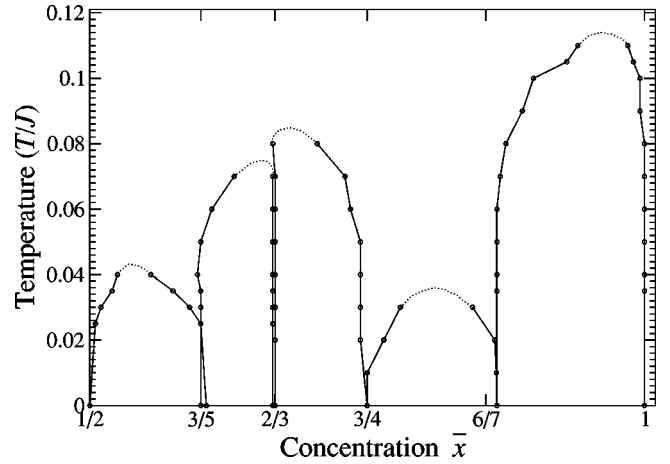


FIG. 15. Phase diagram for the triangular lattice with Coulomb interaction in the region  $x > 1/2$  obtained with MC simulations.

mediate concentrations. When simulations are performed at a constant value of the chemical potential there is no problem connected with background charge that prohibits the phase separation and there is no stress in the system. Thus energies at intermediate concentrations effectively become smaller.

The last reason that we can mention is the local character of the  $A$  and  $B$  operations that were used to introduce changes in the system. Their local character can also become important at low temperatures.

All the reasons discussed above can lead to larger regions of stability for concentrations  $x = 1/4$ ,  $1/2$ , and  $3/4$  and to smaller regions of stability for concentrations  $x = 1/3$  and  $x = 2/3$ . They also explain the appearance of concentrations  $x = 2/5$  and  $x = 3/5$ .

One can obtain the phase diagram for the triangular lattice in the same way as for the linear chain. In order to obtain the phase diagram of the system at low temperature we had to perform up to 100 000 MC sweeps on the lattice with the sample size equal to  $30 \times 30$ . The phase diagram of the triangular lattice is shown in Fig. 15. Only half of the phase diagram is shown since it is symmetric with respect to  $x = 1/2$ . There are five distinct regions of phase separation that correspond to the transitions in concentrations  $1/2 \rightarrow 3/5$ ,  $3/5 \rightarrow 2/3$ ,  $2/3 \rightarrow 3/4$ ,  $3/4 \rightarrow 6/7$ , and  $6/7 \rightarrow 1$  at zero temperature. Some regions of phase separation exist only at low temperature and it is difficult to obtain an accurate phase boundary for them.

## VI. CONCLUSION

We have introduced and studied a model to describe the possible ion orderings in layered double hydroxides. In the model, ions situated at the sites of the triangular lattice interact through long-range Coulomb interaction. The exactly solvable example of the linear chain was used to obtain insight into the model properties and to demonstrate the precision of the MC simulation methods employed. The model predicts multiple phase transitions and phase-separation regions.

Our results are in agreement with experimental measurements in the sense that concentrations  $x = 1/4$  and  $x = 1/3$  are

special.<sup>2-6</sup> However, a large number of predicted possible phases with different fractions of metal ions can lead to the situation in which effects are hard to see in experiments. If we assume that some phase separation occurs, then we should allow for the fact that there are different amounts of  $[\text{CO}_3]^{2-}$  anions in the different regions of the same gallery. Regions with a large number of  $[\text{CO}_3]^{2-}$  anions should have a larger interlayer spacing than regions with a small number of  $[\text{CO}_3]^{2-}$  anions. This should lead to mechanical stress in the system, and that will also resist the tendency to phase separate. This competition between the Coulomb tendency to phase separate and mechanical stress can lead to the disintegration of the compounds and limit the composition range over which layered hydroxides can be synthesized. However, the effect of nonzero temperature can move the system, over the phase-separation boundary and bring the system to a uniform distribution of charges. In this case there should be no

internal stress in the compounds. Thus Al-substituted layered-Ni hydroxides that are stable at higher temperatures may become unstable and disintegrate at lower temperatures.

It would be interesting to see detailed experimental measurements that can support evidence for the charge ordering and the presence or absence of phase separation in these systems.

#### ACKNOWLEDGMENTS

We would like to thank M.V. Chubynsky, S.D. Mahanti, J.B. Parkinson, and T.J. Pinnavaia for several very useful discussions. B.W.S. would like to thank Michigan State University for its kind hospitality during a sabbatical leave. The work was supported by the NSF-CRG Grant No. CHE-0211029 and the Natural Sciences and Engineering Research Council of Canada.

- 
- <sup>1</sup>Y. Xiao, M.F. Thorpe, and J.B. Parkinson, Phys. Rev. B **59**, 277 (1999).
- <sup>2</sup>H.F.W. Taylor, Miner. Mag. **39**, 377 (1973).
- <sup>3</sup>D.L. Bish and G.W. Brindley, Am. Mineral. **62**, 458 (1977).
- <sup>4</sup>G.W. Brindley and S. Kikkawa, Am. Mineral. **64**, 836 (1979).
- <sup>5</sup>S.A. Solin, D.R. Hines, G.T. Seidler, and M.M.J. Treacy, J. Phys. Chem. Solids **57**, 1043 (1996).
- <sup>6</sup>D.R. Hines, G.T. Seidler, M.M.J. Treacy, and S.A. Solin, Solid State Commun. **101**, 835 (1997).
- <sup>7</sup>S.A. Solin, D.R. Hines, S.K. Yuk, T.J. Pinnavaia, and M.F. Thorpe, J. Non-Cryst. Solids **182**, 212 (1995).
- <sup>8</sup>A. Audemer, A. Delahaye, R. Farhi, N. SacEpee, and J.M. Tarascon, J. Electrochem. Soc. **144**, 2614 (1997).
- <sup>9</sup>S.U. Falk and A.J. Salkind, *Alkaline Storage Batteries* (Wiley, New York, 1969).
- <sup>10</sup>R. Barnard and C.F. Randell, J. Appl. Electrochem. **13**, 97 (1983).
- <sup>11</sup>A.D. Vidal and M. Figlarz, J. Appl. Electrochem. **17**, 589 (1987).
- <sup>12</sup>P. Elumalai, H.N. Vasan, and N. Munichandraiah, J. Power Sources **93**, 201 (2001).
- <sup>13</sup>B. Liu, X.Y. Wang, H.T. Yuan, Y.S. Zhang, D.Y. Song, and Z.X. Zhou, J. Appl. Electrochem. **29**, 855 (1999).
- <sup>14</sup>C. Faure, C. Delmas, and P. Willmann, J. Power Sources **36**, 497 (1991).
- <sup>15</sup>G.A. Caravaggio, C. Detellier, and Z. Wronski, J. Mater. Chem. **11**, 912 (2001).
- <sup>16</sup>F. Ducastelle, *Order and Phase Stability in Alloys* (Elsevier Science, Amsterdam, 1991).
- <sup>17</sup>A.J. Berlinsky, W.G. Unruh, W.R. McKinnon, and R.R. Haering, Solid State Commun. **31**, 135 (1979).
- <sup>18</sup>W. Li, J.N. Reimers, and J.R. Dahn, Phys. Rev. B **46**, 3236 (1992).
- <sup>19</sup>A.H. Thompson, J. Electrochem. Soc. **126**, 608 (1979).
- <sup>20</sup>M. Winter, J.O. Besenhard, M.E. Spahr, and P. Novak, Adv. Mater. (Weinheim, Ger.) **10**, 725 (1998).
- <sup>21</sup>T. Zheng and J.R. Dahn, Phys. Rev. B **56**, 3800 (1997).
- <sup>22</sup>S.A. Safran and D.R. Hamann, Phys. Rev. B **22**, 606 (1980).
- <sup>23</sup>S.A. Safran and D.R. Hamann, Phys. Rev. Lett. **42**, 1410 (1979).
- <sup>24</sup>H.A. Kramers and G.H. Wannier, Phys. Rev. **60**, 252 (1941).
- <sup>25</sup>M.E.J. Newman and G.T. Barkema, *Monte Carlo Methods in Statistical Physics* (Oxford University, New York, 1999).
- <sup>26</sup>A.C. Maggs and V. Rossetto, Phys. Rev. Lett. **88**, 196402 (2002).
- <sup>27</sup>E.P. Wigner, Phys. Rev. **46**, 1002 (1934).
- <sup>28</sup>G. Meissner, H. Namaizawa, and M. Voss, Phys. Rev. B **13**, 4 (1976).
- <sup>29</sup>L. Bonsall and A.A. Maradudin, Phys. Rev. B **15**, 1959 (1977).
- <sup>30</sup>This exact result only agrees with the approximate expression in Eq. (11) of Ref. 1 in the limit  $x \rightarrow 0$ .